Analysis & Sensing

Research Article
doi.org/10.1002/anse.202200049

Chemistry Europe
European Chemical Societies Publishing

www.analysis-sensing.org

Special Collection

Isothermal Rolling Circle Amplification and Lanthanide-Based FRET for Femtomolar Quantification of MicroRNA

Mariia Dekaliuk,[a] Pierre Busson,[b] and Niko Hildebrandt*[a, c]

Quantification of DNA and RNA biomarkers via isothermal amplification technologies can significantly simplify biosensing and clinical diagnostics. However, highly sensitive and wash-free assay formats based on time-resolved Förster resonance energy transfer (TR-FRET) have been limited to terbium (Tb) based FRET pairs and their application on specialized clinical instruments. Here, we present the implementation of rolling circle amplification (RCA)-FRET to europium-dye (Eu-ATTO620) FRET pairs and its application on standard benchtop fluorescence plate readers. Eu-ATTO620 RCA-FRET was used to quantify microRNA-21 (miR-21) in a 1 to 100 pM concentration range on a SPARK multimode plate reader system. Detection limits down to 120 ± 20 fM (18 ± 3 attomol of miR-21) and quantification of endogenous miR-21 from the plasma of ovarian cancer patients using a KRYPTOR clinical plate reader demonstrated the broad applicability and clinical relevance of Eu-dye-based RCA-FRET. The extension to both Eu and Tb based TR-FRET and to standard bioanalytical laboratory instruments has the potential to significantly broaden the application and versatility of RCA-FRET for simple, highly-sensitive, and multiplexed bioanalysis.

Introduction

Isothermal amplification of DNA has become an almost unlimited toolbox of techniques to quantify DNA, RNA, and other, non-nucleic acid biomarkers at ultralow concentrations without the necessity of thermal cycling.[1–4] Among the most popular approaches for biosensing are loop-mediated isothermal amplification (LAMP)[5,6] for exponential and rolling circle amplification (RCA)[7,8] for linear amplification. The versatility of amplification approaches can be combined with a large choice of signal transduction methods, including gel electrophoresis, colorimetry, plasmon resonance, electrochemistry, and luminescence.[1,4,9,10] On the way to clinical translation,[11] new materials (e.g., nanomaterials)[12] and miniaturization (e.g., microfluidic devices)[13] have also played an important role for advancing isothermal DNA amplification methods.[9] The COVID-19 pandemic has resulted in an additional exponential growth of the interest in isothermal amplification techniques for rapid and simple diagnosis.[14] However, traditional reverse-transcription quantitative polymerase chain reaction (RT-qPCR) largely remains the method of choice. This example shows that methodology development efforts for biological analysis and sensing are often directed toward novelty and impact and to a lesser extend toward advancement, optimization, adaption, and broadening of existing methods, such that they can be used by a broad community of researchers for actual biosensing.

One possibility of improving simplicity and sensitivity of biosensors is the application of Förster resonance energy transfer (FRET).[15] FRET requires the interaction of a donor-acceptor pair within a distance of approximately 1 to 10 nm, which can be implemented into specific biological recognition and thereby avoid any washing or separation steps within biological assays.[16] FRET with different fluorophores, such as dyes or quantum dots, has also been implemented into isothermal amplification for biosensing.[17–22] Time-resolved (TR) or time-gated (TG) FRET with long-lifetime luminescent lanthanide complexes can be exploited to reduce background from autofluorescence and directly excited acceptors and thereby further decrease detection limits and increase sensitivity.[23,24] We recently merged TG-FRET and RCA to develop isothermal and multiplexed biosensors for DNA and RNA.[25–27] Compared to conventional methods, such as RT-qPCR, RCA-FRET is significantly simpler (isothermal amplification), wash-free (separation of non-hybridized FRET probes is not necessary), more specific (single-nucleotide variation distinction at varying positions within the target), more precise (narrower distribution of concentrations and better distinction between healthy and pathological samples), and provides a rapid, ratiometric, and single-step detection format for sensitive quantification of microRNAs from different clinical samples, including blood, cells, and tissue.[26]

[a] Dr. M. Dekaliuk, Prof. Dr. N. Hildebrandt
nanoFRET.com, Laboratoire COBRA (UMR6014 & FR3038)
Université de Rouen Normandie, CNRS, INSA
Normandie Université, 76000 Rouen (France)
E-mail: niko.hildebrandt@univ-rouen.fr
[b] Dr. P. Busson
CNRS UMR 9018-METSY
Gustave Roussy and Université Paris-Saclay
94805 Villejuif (France)
[c] Prof. Dr. N. Hildebrandt
Department of Chemistry
Seoul National University
Seoul 08826 (South Korea)

Supporting information for this article is available on the WWW under https://doi.org/10.1002/anse.202200049

Special Collection *This article is part of a Special Collection on luminescence sensing.*

Despite these benefits, TG RCA-FRET biosensors were developed only for Tb complexes and their application was limited to a specific clinical plate reader system. This is somewhat disadvantageous because other lanthanide, in particular Eu-based, complexes are very often applied in biosensing,[28–31] including their use on standard benchtop fluorescence plate readers that are equipped with TR-FRET or HTRF (homogeneous time-resolved fluorescence) functionality, such as platforms from (in alphabetical order) Berthold, BioTek, BMG Labtech, Molecular Devices, Perkin-Elmer, Promega, SAFAS, Tecan, or ThermoFisher, to name only a few. In order to make the amplified TR-FRET sensing technology available to a broader user community, demonstration of assays with Tb and Eu on different plate reader systems is clearly necessary.

Here, we present the application of two independent lanthanide-dye FRET pairs, namely Lumi4-Tb (Tb) plus Cy5.5 and Lumi804-Eu (Eu) plus ATTO620, for the quantification of microRNA-21 (miR-21) as prototypical biomarker using RCA-FRET. We first optimized the RCA-FRET protocol, for which we tested different buffer compositions and polymerases, and then applied both assays to a KRYPTOR compact PLUS (Thermo Fisher Scientific)[32] clinical plate reader and a SPARK (Tecan)[33] multimode plate reader to evaluate their sensing performances. Both FRET pairs could quantify miR-21 in a circa 1 to 100 pM concentration range on both plate reader systems. Although the sensitivities of the new Eu-ATTO620 FRET pair was approximately 75-fold lower compared to Tb-Cy5.5, the detection limit was only circa four times higher. To demonstrate the applicability of the new Eu-ATTO620 FRET pair, we quantified endogenous miR-21 in the plasma of ovarian cancer patients, in very good agreement with previous results obtained with the Tb-Cy5.5 FRET pair. Our results show the broad applicability of RCA-TG-FRET with both common lanthanide complexes, which will significantly improve its availability to a broad biosensing community for adaption to other biological targets and other fluorescence reader systems.

Results and Discussion

To demonstrate the broad applicability of RCA-FRET, we investigated the previously used FRET pair of Tb-Cy5.5[25–27] and the new FRET pair of Eu-ATTO620. Both lanthanide complexes were developed by Lumiphore (see Supporting Figure S1 for chemical structures)[34–36] and their NHS-activated complexes were conjugated in house to C6-amino functionalized 5′ termini of DNA probes, whereas the dye acceptors (Cy5.5 from GE Healthcare and ATTO620 from ATTO Technology) were directly purchased as 5′-functionalized DNA from Eurogentec. Absorption and emission spectra are shown in Figure 1A. Both Tb and Eu can be excited in the UV. Tb has a higher extinction coefficient (26,000 $M^{-1}cm^{-1}$ at 340 nm) and Tb-centered quantum yield (0.70 ± 0.05) compared to Eu (14,300 $M^{-1}cm^{-1}$ at 363 nm and 0.49 ± 0.04 Eu-centered quantum yield) but Eu can be excited further in the visible spectral range (toward 400 nm) compared to Tb. Their photoluminescence (PL) spectra overlap well with the acceptor dyes Cy5.5 and ATTO620 and the Tb and Eu quenched PL and Cy5.5 and ATTO620 sensitized PL can be well separated by using transmission filters (cf. Figure 1A). The long PL lifetimes of Tb (~2.7 ms) and Eu (~0.76 ms) allow for efficient suppression of background PL (from sample autofluorescence and directly excited dyes) via pulsed excitation and TG detection in a time window from 0.1 to 0.9 ms after the excitation pulse.[24] Due to FRET from Tb to Cy5.5 or Eu to ATTO620, the FRET-sensitized dyes also emit PL with a long lifetime that can be measured in the same TG detection window.

The RCA-FRET assay principle is shown in Figure 1B. It is based on target-primed RCA of padlock probes, which is a well-established and well-characterized method for nucleic acid identification and quantification in solution and in situ.[7,8,25,37–40] We used miR-21, a frequently investigated microRNA cancer biomarker,[41,42] as prototypical target because we had previously optimized the assay for miR-21 quantification with the Tb-Cy5.5 FRET pair in plasma extracts from ovarian cancer patients.[26] Within that study, we also demonstrated the significant microRNA specificity advantages of RCA-FRET over RT-qPCR and the possibility of single-nucleotide mismatch detection.[26] Other microRNA or DNA targets as well as deoxyribonucleoside triphosphates can also be detected with the same RCA-FRET technology.[25–27,43] Upon target-padlock hybridization, the padlock is circularized, followed by target-primed RCA. FRET probes are then hybridized to the RCA product, which results in approximately a thousand FRET pairs per miR-21 target. Because only hybridization of both donor (Tb or Eu) and acceptor (Cy5.5 or ATTO620) probes to the RCA product can result in FRET (in solution the FRET probes are not within sufficient distance for FRET), the detection technology is wash and separation free. Within the RCA product, the donor-acceptor distance is 18 nucleotides, which corresponds to circa 6 nm donor-acceptor distance (assuming ~0.33 nm per base pair).[44] This distance is close to the Förster distance (distance with 50% FRET efficiency) of the two FRET pairs (5.8 ± 0.2 nm for Tb-Cy5.5 and 6.9 ± 0.3 nm for Eu-ATTO620) and therefore well suited for TG-FRET analysis.

Because RCA-FRET was previously shown and optimized only with Tb donors and only on a specialized clinical plate reader (KRYPTOR), we sought to demonstrate a generic use with Eu donors also and application on a standard benchtop multimode fluorescence plate reader. Thus, we quantified miR-21 in a concentration range from 0.2 to 10 pM using both KRYPTOR and SPARK readers. Before this comparison, we also tested different buffer conditions and DNA polymerases. We found especially that the ATP concentration in the buffer was influencing the assay performance (see Experimental Section for details) and that Phi29 DNA polymerase was better suited for RCA-FRET compared to EquiPhi29 DNA polymerase, despite the allegedly accelerated RCA production as advertised by the supplier (Supporting Figure S2).

Both plate readers used the same 96-well microtiter plates with a total measuring volume of 140 μL per well and performed pulsed excitation (337 nm) and TG detection (0.1 to 0.9 ms after excitation for KRYPTOR and 0.1 to 2.1 ms after excitation for SPARK) of both donor and acceptor PL (for

Research Article
doi.org/10.1002/anse.202200049
Chemistry Europe
European Chemical Societies Publishing

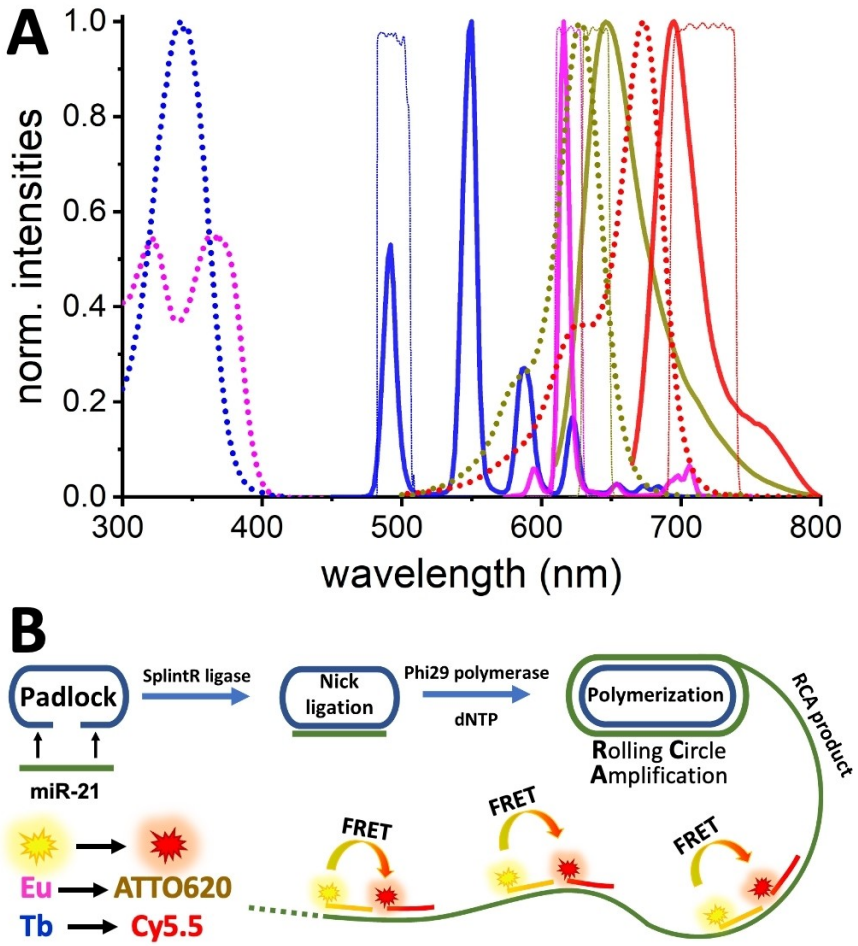

Figure 1. A) Absorption (dotted lines) and PL (full lines) spectra of the FRET donors (Tb and Eu) and acceptors (Cy5.5 and ATTO620) used for RCA-FRET assays (Tb: blue; Eu: magenta; ATTO620: dark yellow; Cy5.5: red). Transmission spectra of the emission filters are shown as thin lines in the background. **B)** Schematic principle of RCA-FRET assays, which include four main stages, namely padlock-target recognition, nick ligation, polymerization, and FRET probe hybridization.

details, see Experimental Section). The *FRET ratio* (ratio of acceptor and donor PL signals) was used as signal for quantifying the miR-21 concentrations (Figure 2). Under optimized buffer and polymerase conditions, both instruments showed a miR-21 concentration dependent increase of the *FRET ratio* with the strongest dynamic signal in a concentration range from circa 1 to 10 pM. The sensitivities (ΔS, slopes of the calibration curves in the linear 1 to 10 pM concentration range) were relatively similar for both instruments, which means that they could both very well distinguish miR-21 concentrations in the 1 to 10 pM concentration range. However, the signal deviations (error bars) were significantly larger for the SPARK reader, which means that distinguishing miR-21 concentrations, in particular at very low concentrations, was easier for the KRYPTOR. This was somewhat expected, considering that the KRYPTOR used laser excitation and filter-based wavelength separation, whereas the SPARK used a flash lamp and monochromator-based spectral filtering.

Independent of the instruments, the assay sensitivity was significantly better (approximately 70 to 80 fold) when using the Tb-Cy5.5 FRET pair: ΔS(Tb-Cy5.5, KRYPTOR) = 3.9 ± 0.4 pM^{-1}, ΔS(Tb-Cy5.5, SPARK) = 3.0 ± 0.3 pM^{-1}, ΔS(Eu-

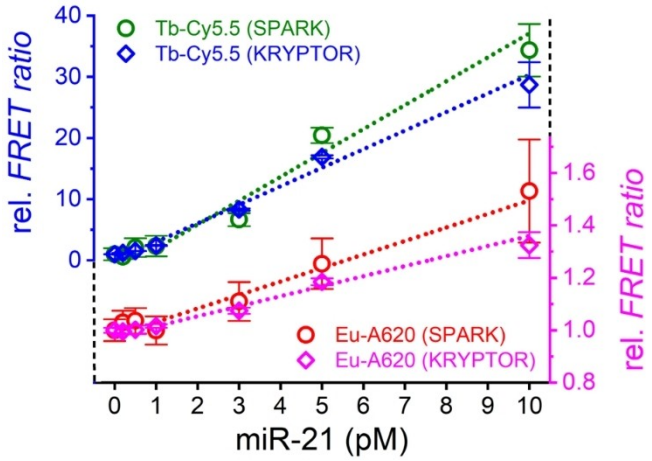

Figure 2. RCA-FRET assay calibration curves for quantifying miR-21 with the two different FRET pairs (Tb-Cy5.5 and Eu-ATTO620) on two different plate readers (KRYPTOR and SPARK). Note that all concentrations correspond to those in the 150 µL total assay volume from which 140 µL were used for the measurements. Concentrations in the 5 µL sample volume were 30-fold higher. Error bars represent standard deviations from four independent measurements.

Research Article
doi.org/10.1002/anse.202200049
Chemistry Europe
European Chemical Societies Publishing

ATTO620, KRYPTOR) = 0.052 ± 0.005 pM^{-1}, ΔS(Eu-ATTO620, SPARK) = 0.038 ± 0.004 pM^{-1}. Although the Eu-ATTO620 Förster radius is slightly larger compared to Tb-Cy5.5 (see above), the difference in sensitivity was mainly caused by three distinct properties of the FRET assays. First, for comparison, we used the same excitation wavelength of 337 nm (which is a fixed wavelength for the KRYPTOR laser) for both FRET pairs and Tb has a more than 2-fold higher absorption cross section at this wavelength compared to Eu (cf. Figure 1A). Notably, at wavelengths above 370 nm, which may be useful for imaging applications, the Eu complex has a better absorption compared to Tb. Second, the spectral distinction of Tb and Cy5.5 PL is very efficient and there is only negligible spectral crosstalk in the Tb and Cy5.5 detection channels (blue and red PL and filter transmission spectra in Figure 1A). For Eu and ATTO620 (magenta and dark yellow PL and filter transmission spectra in Figure 1A) spectral separation is more complicated with significant spectral crosstalk. Third, the spectral detection range of the Cy5.5 dye is larger (red filter transmission spectrum in Figure 1A) due to the negligible spectral contribution of Tb beyond 700 nm, which means that more acceptor photons can be detected. At very low concentrations (below 1 pM) the Tb-Cy5.5 FRET pair showed a slight signal increase, whereas the Eu-ATTO620 FRET pair showed a fluctuating signal independent of the miR-21 concentration. To investigate these low concentrations, we scrutinized the new Eu-ATTO620 FRET pair in more detail using the KRYPTOR reader.

The miR-21 assay calibration curve (Figure 3A) shows a relatively broad dynamic range (~0.5 to 100 pM) for a wash-free FRET assay with the typical saturation at high target concentrations. The limit of detection (LOD) was determined on the calibration curve as three standard deviations (3σ) above the zero-concentration *FRET ratio* using various miR-21 concentrations in the sub-pM concentration range (Figure 3B). While the sensitivity was lower in this concentration range, there was a clear miR-21 concentration dependent *FRET ratio* increase and the LOD was 120 ± 20 fM. This LOD represents the detection limit of the assay with a total assay volume of 150 µL (from which 140 µL are used for the measurement). The LOD in the 5 µL sample (contained within the 150 µL assay volume) was 30-fold higher (3.6 ± 0.6 pM). The volume-independent LOD was 18 ± 3 attomol of miR-21. Assay volume reduction may further decrease the molar LOD. However, the KRYPTOR immunoassay plate reader system is currently optimized for 96-well plates with an assay volume of ~150 µL. Despite the approximately four-fold higher LOD compared to the Tb-Cy5.5 FRET pair (30 ± 3 fM or 4.5 ± 0.5 attomol), the concentration should still be sufficiently low to quantify microRNAs from real clinical samples.

To evaluate the applicability of the new Eu-ATTO620 FRET pair for quantifying microRNAs from real clinical samples, we used small RNA extracts from the plasma of six ovarian cancer patients. In a previous study using the Tb-Cy5.5 FRET pair and RT-qPCR as comparative method to evaluate miR-21 concentrations in plasma samples of ovarian cancer patients and healthy persons, we could establish a threshold concentration

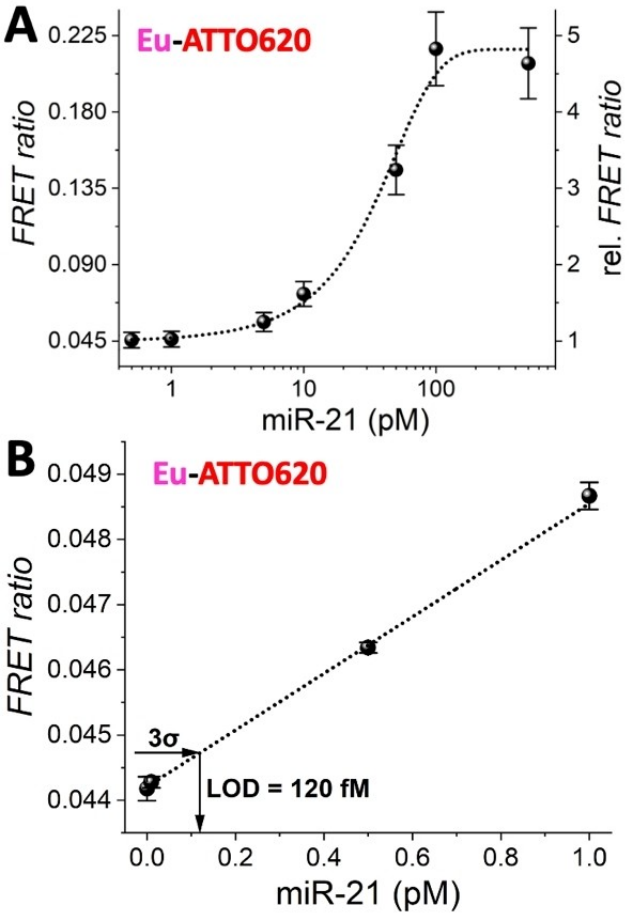

Figure 3. A) RCA-FRET calibration curve for the Eu-ATTO620 FRET pair applied to the KRYPTOR plate reader. **B)** Determination of the LOD using miR-21 concentrations in the sub pM concentration range. Note that all concentrations correspond to those in the 150 µL total assay volume. Concentrations in the 5 µL sample volume were 30-fold higher. Error bars represent standard deviations from three (10 for the zero concentration control sample in B) independent measurements.

of 0.153×10^6 copies of miR-21 per ng of small RNA, above which the probability for ovarian cancer was ~62% (~38% of the ovarian cancer patient plasma samples showed concentrations below the threshold) when using RCA-FRET.[26] Taking into account that the aim of our current study was the demonstration of applicability of the Eu-ATTO620 FRET pair to real samples, we considered six independent samples as sufficient. Using the established Eu-ATTO620 miR-21 calibration curves and the KRYPTOR clinical plate reader, we quantified the endogenous miR-21 concentrations from the small RNA plasma extracts in the six different samples (Figure 4). Because the molar concentrations of miR-21 (Figure 4A) are independent of the concentration of extracted small RNA, we also normalized the miR-21 concentrations to show the number of miR-21 copies per ng of small RNA (Figure 4B), as done in our previous study (see above). Five of the six ovarian cancer patient samples (83%) showed a miR-21 concentration above the threshold, which was in good agreement with our previous study. Notably, the sample with the miR-21 concentration below the threshold (sample 6) had a very high concentration

Research Article
doi.org/10.1002/anse.202200049

Chemistry Europe
European Chemical Societies Publishing

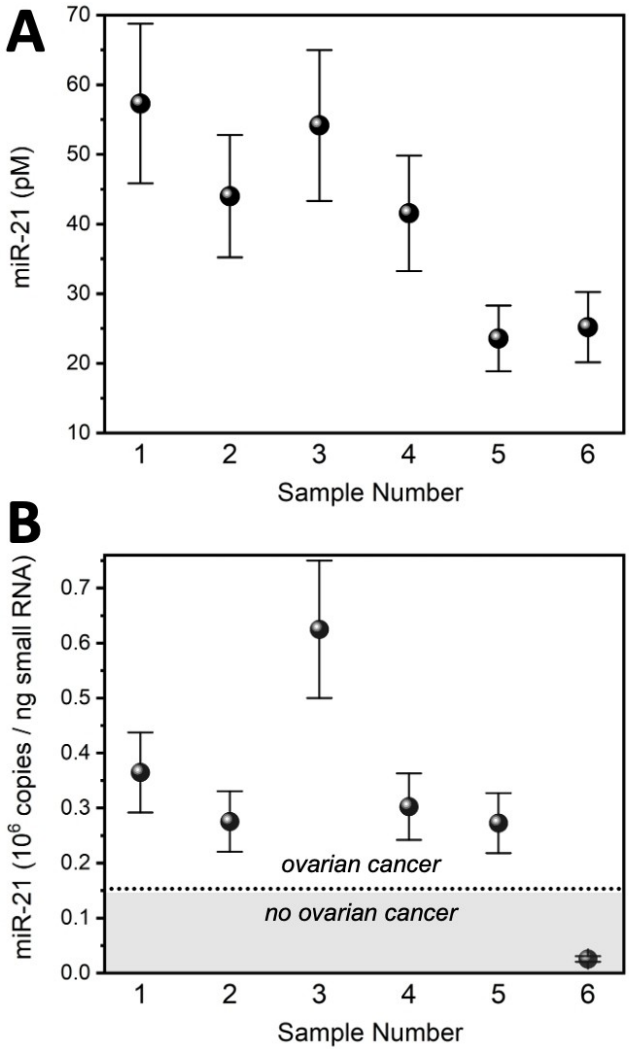

Figure 4. Quantification of endogenous miR-21 from real clinical samples. **A**: Molar concentrations in the 5 µL plasma extracted small RNA samples. **B**: Concentrations in miR-21 copies per ng of small RNA). Samples 1 to 6 were from ovarian cancer patients. The dotted line at 0.153×10^6 copies/ng small RNA corresponds to a threshold concentration to distinguish between ovarian cancer (above) and healthy controls (below) as previously found for a study with a larger amount of patients and samples.[26] Error bars represent 20% estimated error for concentration recovery.

of small RNA after plasma extraction and it may be interesting to evaluate the influence of small RNA concentration on the quantification of microRNAs on larger sample cohorts in the future. However, considering the limited amount of patient samples, it would be more reasonable to use the higher-sensitivity Tb-Cy5.5 FRET pair for such investigations. Still, the Eu-ATTO620 results clearly showed that endogenous miR-21 could be quantified from real clinical samples.

Conclusions

In this study, we have demonstrated the successful implementation of time-resolved or time-gated RCA-FRET for Eu-based FRET pairs and the application on standard benchtop fluorescence plate readers. Although the Tb-Cy5.5 FRET pair provided the best assay performance regarding both sensitivity and detection limit, the LOD of the Eu-ATTO620 FRET pair was only ~4-fold higher, which corresponds to other Tb-based FRET pairs, such as Tb-Cy3.5.[25] Concerning instruments, the clinical plate reader KRYPTOR (Thermo Fisher Scientific) provided the best assay performance. However, both Tb and Eu based FRET pairs could quantify miR-21 in a low pM concentration range on a SPARK (Tecan) multimode fluorescence plate reader. Real-sample applicability was demonstrated by quantifying endogenous miR-21 from plasma extracts of ovarian cancer patients. Our results demonstrate the broad applicability of RCA-FRET, such that this sensitive and wash-free biosensing technology can be easily adapted by different labs with standard materials and standard equipment to analyze different nucleic acid biomarkers. In future studies, it would be highly interesting to investigate the multiplexing potential because Eu-based FRET pairs are both spectrally and temporally distinct from Tb-based FRET pairs, which could be potentially exploitable for higher-order multiplexed biosensing.[24,25,45–48] Additionally, adapting instruments to smaller detection volumes has the potential to further improve the assay performance, which may be highly beneficial to detect trace amounts of minimally expressed biomarkers in clinical samples and to advance RCA-FRET toward point-of-care testing. Overall, there is a large potential to further improve and optimize RCA-FRET toward a standard bioanalytical method for sensitive, simple, and wash-free quantification of nucleic acids and other biomarkers.

Experimental Section

Materials

Reagents: Lumi804-Eu-NHS and Lumi4-Tb-NHS (Lumiphore); Nuclease free water (New England BioLabs); Phi29 DNA Polymerase (10×, New England BioLabs) – store at −20 °C; Phi29 DNA polymerase reaction buffer (10×, New England BioLabs), included in Phi29 DNA Polymerase set, 1×: 50 mM Tris-Cl, 10 mM $MgCl_2$, 10 mM $(NH_4)_2SO_4$, 4 mM DTT, pH 7.5 at 25 °C – store at −20 °C and avoid freeze-thaw cycles; Sodium chloride (Sigma Aldrich); SplintR ligase (25000 U ml^{-1}; New England BioLabs), included in SplintR ligase set – store at −20 °C; SplintR ligase buffer (10×, New England BioLabs), included in SplintR ligase set, 1×: 50 mM Tris-HCl, 10 mM $MgCl_2$, 1 mM ATP, 10 mM DTT, pH 7.5 at 25 °C – should be adjusted before use in RCA-FRET (see "Buffers" below), store at −20 °C and avoid freeze-thaw cycles; T4 RNA ligase buffer (10×, News England Biolabs), 1×: 50 mM Tris-HCl, 10 mM $MgCl_2$, 1 mM DTT, pH 7.5 at 25 °C – should be adjusted before use in RCA-FRET (see "Buffers" below); Synthetic oligonucleotides: miR-21, padlock probe, luminescent probes (Eurogentec) – store at −20 °C and avoid freeze-thaw cycles, for long-term storage −80 °C is recommended; Trizma® hydrochloride (Sigma Aldrich); HEPES (Sigma Aldrich); Sodium bicarbonate (Sigma Aldrich); Sodium carbonate (Sigma Aldrich); Deoxynucleotide (dNTP) Solution Mix (10 mM, New England BioLabs), a ratio of 1:1:1:1 dATP:dTTP:dCTP:dGTP was used – store at −20 °C and avoid freeze-thaw cycles; Millipore ultrapurified water (Milli-Q).

Nucleic acid probes and exogenous target: All sequences and modifications of synthetic oligonucleotide probes are summarized in Table 1. Lumi4-Tb-NHS (Tb-NHS) and Lumi804-Eu-NHS (Eu-NHS)

Research Article
doi.org/10.1002/anse.202200049

Chemistry Europe
European Chemical Societies Publishing

Table 1. Sequences and modifications of miR-21 and different DNA probes. Target specific area of the padlock to the target shown in *italic*. Eu/Tb probe complementary sequence shown in **bold**. A620 and Cy5.5 complementary sequences are underlined.

Probe name	Sequence 5′-3′	Modification
miR-21	UAG CUU AUC AGA CUG AUG UUGA	
padlock probe	*TGA TAA GCT A*AT ATA TGA TGG **AAT CAA GAC AAT ATT GTT** GAT GCC GAA TTT TTC AAG AGG AAA TGT *TCA ACA TCA GTC*	5′-Phosphate
Eu probe/ Tb probe	**AAT CAA GAC AAT ATT GTT**	5′-C6 amino
A620 probe	GAT GCC GAA TTT TTC AAG AG	5′-ATTO620
Cy5.5 probe	GAT GCC GAA TTT TTC AAG AG	5′-Cy5.5

oligo conjugation was performed as described elsewhere.[49] Briefly, a mixture of 2.1 μL of Tb-NHS or Eu-NHS (8 mM), 10 μL of amino-functionalized oligonucleotide (100 μM), and 7.9 μL of carbonate buffer (100 mM) were incubated overnight at 4 °C. The Tb or Eu oligo conjugate was purified three times with 100 mM HEPES buffer by Zeba Spin Desalting Columns (7 kDa molecular weight cutoff). Tb and Eu and oligo concentrations were determined by absorbance measurement at 340 nm (Tb, 26,000 $M^{-1}cm^{-1}$), 363 nm (Eu, 14,300 $M^{-1}cm^{-1}$), and 260 nm (DNA, 187,500 $M^{-1}cm^{-1}$), respectively. Conjugation ratios were determined by a linear combination of the respective absorbance values of Tb or Eu and oligo within Tb and Eu oligo conjugates. All ratios were higher than 0.85 Tb/oligo or Eu/oligo.

Buffers: Buffer 1a: Adapted SplintR ligase buffer (50 mM Tris-HCl, 10 mM $MgCl_2$, 1 mM ATP, 10 mM DTT, 100 mM NaCl, pH 7.5 at 25 °C); Buffer 1b: Adapted T4 RNA ligase buffer (50 mM Tris-HCl, 10 mM $MgCl_2$, 1 mM DTT, 10 μM ATP, 100 mM NaCl, pH 7.5 at 25 °C); Buffer 2: 1× Phi29 DNA polymerase reaction buffer; Buffer 3: 20 mM Tris-Cl, 500 mM NaCl, 0.1% BSA, pH 8.0 at 25 °C; 100 mM carbonate buffer, pH 9.0 at 25 °C; 100 mM HEPES buffer, pH 7.4 at 25 °C.

Methods

Förster distance (R_0) determination: R_0 (donor-acceptor distance for which FRET efficiency is 50%) of the Eu–A620 FRET pair (6.9 ± 0.3 nm) was calculated using the following equations: (1) $R_0 = 0.021 (\kappa^2\ \Phi_D\ n^{-4}\ J)^{1/6}$ nm; (2) $J = \int_{500nm}^{750nm} I_D(\lambda)\ \varepsilon_A(\lambda)\ \lambda^4\ d\lambda$. A dipole-dipole orientation factor (κ^2) of 2/3 was assumed, as justified by the random orientation of donor and acceptor during the FRET time (dynamic averaging) taking into account the long PL lifetime of the Eu donor and its unpolarized emission. The Eu-centered quantum yield (Φ_D) was 0.49. For aqueous solutions, the refractive index of the medium (n) was taken as 1.35. The overlap integral (J) was calculated by the spectral overlap between the area normalized (to unity) PL spectrum of Eu (the entire spectrum between 500 and 750 nm) and the molar absorptivity spectrum of the ATTO620 ($\varepsilon_{max} = 125{,}000\ M^{-1}cm^{-1}$) from 500 to 750 nm. R_0 of Tb-Cy5.5 (5.8 ± 0.2 nm) was determined previously.[26]

RCA-FRET assay preparation: All assays were prepared on a clean bench. For a typical assay, 5 μL of 30 nM padlock probe and 5 μL of miR-21 in various concentrations (depending on the assay calibration curve) were prepared in Buffer 1a. The mixture was incubated in a thermal cycler at 80 °C for 2 min followed by a decrease to 22 °C with 2 °C min^{-1} speed. Then, 21.5 U of SplintR ligase in 5 μL Buffer 1a was added to the mixture and incubated at 37 °C for 1 h. Afterwards, a mixture of 5 U of phi29 DNA polymerase and 2 mM dNTP prepared in 15 μL of Buffer 2 was added and incubated at 37 °C for 2 h. A mixture of 12.5 nM Eu probe (or 2.5 nM Tb probe) and 12.5 nM ATTO620 probe (or 2.5 nM Cy5.5 probe) was prepared in 120 μL of Buffer 3 and added to the polymerisation mixture without delay. Then, the mixture was incubated in a thermal cycler at 65 °C for 10 min with followed by a decrease to 22 °C with 2 °C min^{-1} speed. From the total reaction volume of 150 μL, 140 μL were transferred to black 96-well microtiter plates.

RCA-FRET assay measurement: TG-FRET measurements were performed on the clinical immunofluorescence plate reader KRYPTOR compact PLUS (Thermo Fisher Scientific) or on the multimode fluorescence plate reader SPARK (Tecan). KRYPTOR: Excitation at 337.1 nm used an integrated nitrogen laser operating at 20 Hz with 100 pulses. The time delay of 0.1 ms, detection window time of 0.8 ms, and excitation with 100 pulses were selected to efficiently suppress all short-lifetime background. TG PL intensities were detected using bandpass filters 620 ± 7 nm for Eu detection channel, 640 ± 7 nm for ATTO620 detection channel, 494 ± 12 nm for Tb detection channel, and 716 ± 20 nm for Cy5.5 detection channel. SPARK: Excitation wavelength: 337 nm with a bandwidth of 20 nm; Emission wavelengths: Eu: 620 nm, bandwidth 5 nm, gain 160; ATTO620: 640 nm, bandwidth 5 nm, gain 180; Tb: 494 nm, bandwidth 5 nm, gain 180; Cy5.5: 718 nm, bandwidth 5, gain 180. Integration time: 2 ms, lag time: 0.1 ms. For the KRYPTOR and SPARK comparison tests, the same experimental plate was measured sequentially using both instruments.

Complete RCA-FRET procedure overview: Design of DNA sequences: circa 2–3 h; Order of DNA/RNA oligos: circa 7 to 10 days for delivery; Preparation of oligos for assays: circa 1 h; Conjugation of Tb or Eu to the oligos: circa 10 min + overnight incubation + 30 min; Concentration estimation of the lanthanide-oligonucleotide conjugates (spectroscopy measurement): circa 30 min; RCA: circa 5 h 45 min as follows: i) Target-padlock annealing (~1 h 15 min), ii) Padlock ligation (~1 h 15 min); iii) Polymerization (~2 h); iv) RCA product labeling (~1 h 15 min); v) TG-FRET measurements (10 min instrument setup + 5 min measurement + 10 min data analysis).

Quantification of miR-21 from plasma extracts: All plasma samples were collected from anonymized patients with written informed consent under an agreement of the responsible ethical committees (official permission no. 180510 by the "comité de protection des personnes CPP Sud-Méditerranée IV"). For total RNA extraction, miRNeasy Serum/Plasma Kit (Qiagen) was used and the extraction was performed according to the manufacturer's instructions. The total RNA extract was eluted in 14 μL of nuclease-free water and RNA concentrations were measured using a BMG UV/Vis spectrometer (spectrophotometric quantification of RNA protocol, Qiagen). Small RNA concentrations were 94.6 ng/μL (sample 1), 96.1 ng/μL (sample 2), 52.2 ng/μL (sample 3), 82.7 ng/μL (sample 4), 52.0 ng/μL (sample 5), and 596.5 ng/μL (sample 6). The RCA-FRET assay was prepared as mentioned above by replacing the 5 μL of synthetic miR-21 sample by 5 μL of small RNA plasma extract. The absolute concentrations of miR-21 in the samples were determined using the calibration curves (*FRET ratio*) constructed using synthetic miR-21 with known concentrations (0–10 pM within 150 μL). Concentrations in copies per ng of small RNA were calculated by multiplying the molar amount of miR-21 in the 5 μL sample (as determined in pM multiplied by 5 μL) by Avogadro's number ($6.022\ 10^{23}$) and dividing by the amount (in ng) of small RNA in the 5 μL sample.

Acknowledgements

We thank Lumiphore, Inc. for the gift of Lumi804 and Lumi4 reagents. This work was supported by the Institut National du Cancer and the Direction Générale de l'Offre de Soins (INCa and DGOS; project PRTk 16158 – Gynomir), ITMO Cancer of Aviesan within the framework of the 2021–2030 Cancer Control Strategy through funds administered by Inserm (project "ACTION"), the Brain Pool program funded by the Ministry of Science and ICT through the National Research Foundation of Korea (2021H1D3A2A0204958912), Seoul National University, Université Paris-Saclay, Université de Rouen Normandie, Normandie Université, INSA Rouen, CNRS, European Regional Development Fund, Labex SynOrg (ANR-11-LABX-0029), Carnot Institute I2C, XL-Chem graduate school (ANR-18-EURE-0020 XL-CHEM), and the Région Normandie.

Conflict of Interest

The authors declare no conflict of interest.

Data Availability Statement

The data that support the findings of this study are available in the supplementary material of this article.

Keywords: cancer · DNA · europium · miR-21 · terbium

[1] Y. Zhao, F. Chen, Q. Li, L. Wang, C. Fan, *Chem. Rev.* **2015**, *115*, 12491–12545.
[2] R. Deng, K. Zhang, J. Li, *Acc. Chem. Res.* **2017**, *50*, 1059–1068.
[3] D. M. Nieuwkerk, A. Korajkic, E. L. Valdespino, M. P. Herrmann, V. J. Harwood, *J. Microbiol. Methods* **2020**, *179*, 106099.
[4] J. Glökler, T. S. Lim, J. Ida, M. Frohme, *Crit. Rev. Biochem. Mol. Biol.* **2021**, *56*, 543–586.
[5] K. Shirato, *Microbiol. Immunol.* **2019**, *63*, 407–412.
[6] H. Zhang, Y. Xu, Z. Fohlerova, H. Chang, C. Iliescu, P. Neuzil, *TrAC Trends Anal. Chem.* **2019**, *113*, 44–53.
[7] S. Yue, Y. Li, Z. Qiao, W. Song, S. Bi, *Trends Biotechnol.* **2021**, *39*, 1160–1172.
[8] L. Xu, J. Duan, J. Chen, S. Ding, W. Cheng, *Anal. Chim. Acta* **2021**, *1148*, 238187.
[9] R. Asadi, H. Mollasalehi, *Anal. Biochem.* **2021**, *631*, 114260.
[10] C. Zhang, J. Chen, R. Sun, Z. Huang, Z. Luo, C. Zhou, M. Wu, Y. Duan, Y. Li, *ACS Sens.* **2020**, *5*, 2977–3000.
[11] M. Li, F. Yin, L. Song, X. Mao, F. Li, C. Fan, X. Zuo, Q. Xia, *Chem. Rev.* **2021**, *121*, 10469–10558.
[12] C. Zhang, T. Belwal, Z. Luo, B. Su, X. Lin, *Small* **2022**, *18*, e2102711.
[13] M. C. Giuffrida, G. Spoto, *Biosens. Bioelectron.* **2017**, *90*, 174–186.
[14] We invite the interested reader to perform a search with keywords such as "COVID", "isothermal amplification", "loop-mediated", and "rolling circle amplification" to witness the growth of publications over the last few years.
[15] W. R. Algar, N. Hildebrandt, S. S. Vogel, I. L. Medintz, *Nat. Methods* **2019**, *16*, 815–829.
[16] X. Qiu, N. Hildebrandt, *Expert Rev. Mol. Diagn.* **2019**, *19*, 767–771.
[17] X. Wu, S. Zhu, P. Huang, Y. Chen, *Anal. Biochem.* **2016**, *502*, 16–23.
[18] J. Hu, M.-H. Liu, C.-Y. Zhang, *Chem. Sci.* **2018**, *9*, 4258–4267.
[19] X. Hu, H. Zhang, Y. Zhou, W. Liang, R. Yuan, S. Chen, *Microchim. Acta* **2019**, *186*, 582.
[20] C.-C. Li, J. Hu, X. Luo, J. Hu, C.-Y. Zhang, *Anal. Chem.* **2021**, *93*, 14568–14576.
[21] C. Li, W. Liu, J. Hu, C. Zhang, *Chem. Sci.* **2019**, *10*, 8675–8684.
[22] C. Li, Y. Li, Y. Zhang, C. Zhang, *TrAC Trends Anal. Chem.* **2020**, *122*, 115753.
[23] J. M. Zwier, N. Hildebrandt, in *Reviews in Fluorescence 2016* (Ed.: Geddes, CD), Springer, Cham, **2017**, pp. 17–43.
[24] X. Qiu, J. Xu, M. Cardoso Dos Santos, N. Hildebrandt, *Acc. Chem. Res.* **2022**, *55*, 551–564.
[25] X. Qiu, J. Guo, J. Xu, N. Hildebrandt, *J. Phys. Chem. Lett.* **2018**, *9*, 4379–4384.
[26] X. Qiu, J. Xu, J. Guo, A. Yahia-Ammar, N.-I. Kapetanakis, I. Duroux-Richard, J. J. Unterluggauer, N. Golob-Schwarzl, C. Regeard, C. Uzan, S. Gouy, M. DuBow, J. Haybaeck, F. Apparailly, P. Busson, N. Hildebrandt, *Chem. Sci.* **2018**, *9*, 8046–8055.
[27] M. Dekaliuk, X. Qiu, F. Troalen, P. Busson, N. Hildebrandt, *ACS Sens.* **2019**, *4*, 2786–2793.
[28] J.-C. G. Bünzli, *Coord. Chem. Rev.* **2015**, *293–294*, 19–47.
[29] M. Sy, A. Nonat, N. Hildebrandt, L. J. Charbonniere, *Chem. Commun.* **2016**, *52*, 5080–5095.
[30] J.-C. G. Bünzli, *Eur. J. Inorg. Chem.* **2017**, *2017*, 5058–5063.
[31] L. Francés-Soriano, N. Hildebrandt, L. J. Charbonnière, in *Reference Module in Chemistry, Molecular Sciences and Chemical Engineering*, Elsevier, **2022**.
[32] Thermo Fisher Scientific, "KRYPTOR compact PLUS," can be found under https://www.brahms.de/en-gb/products/kryptor-analyzers/kryptor-compact-plus.html.
[33] Tecan, "Multimode microplate reader, Live cell assays," can be found under https://lifesciences.tecan.com/multimode-plate-reader.
[34] J. Xu, T. M. Corneillie, E. G. Moore, G. L. Law, N. G. Butlin, K. N. Raymond, *J. Am. Chem. Soc.* **2011**, *133*, 19900–19910.
[35] D. Tatum, J. Xu, D. Magda, N. Butlin, *Macrocyclic Ligands with Pendant Chelating Moieties and Complexes Thereof*, **2019**, WO/2019/173639.
[36] A. Foster, S. Nigam, D. S. Tatum, I. Raphael, J. Xu, R. Kumar, E. Plakseychuk, J. D. Latoche, S. Vincze, B. Li, R. Giri, L. H. McCarl, R. Edinger, M. Ak, V. Peddagangireddy, L. M. Foley, T. K. Hitchens, R. R. Colen, I. F. Pollack, A. Panigrahy, D. Magda, C. J. Anderson, W. B. Edwards, G. Kohanbash, *e-biomed* **2021**, *71*, 103571.
[37] J. Banér, M. Nilsson, M. Mendel-Hartvig, U. Landegren, *Nucleic Acids Res.* **1998**, *26*, 5073–5078.
[38] L. Francés-Soriano, M. Leino, M. Cardoso Dos Santos, D. Kovacs, K. E. Borbas, O. Söderberg, N. Hildebrandt, *Anal. Chem.* **2021**, *93*, 1842–1850.
[39] C. Larsson, I. Grundberg, O. Söderberg, M. Nilsson, *Nat. Methods* **2010**, *7*, 395–397.
[40] J. Xu, X. Qiu, N. Hildebrandt, *Nano Lett.* **2021**, *21*, 4802–4808.
[41] "miRCancer – microRNA Cancer Association Database," can be found under http://mircancer.ecu.edu/.
[42] B. Xie, Q. Ding, H. Han, D. Wu, *Bioinformatics* **2013**, *29*, 638–644.
[43] X. Qiu, O. Guittet, C. Mingoes, N. El Banna, M.-E. Huang, M. Lepoivre, N. Hildebrandt, *Anal. Chem.* **2019**, *91*, 14561–14568.
[44] J. Guo, X. Qiu, C. Mingoes, J. R. Deschamps, K. Susumu, I. L. Medintz, N. Hildebrandt, *ACS Nano* **2019**, *13*, 505–514.
[45] C. Chen, L. Ao, Y.-T. Wu, V. Cifliku, M. Cardoso Dos Santos, E. Bourrier, M. Delbianco, D. Parker, J. M. Zwier, L. Huang, N. Hildebrandt, *Angew. Chem. Int. Ed.* **2018**, *57*, 13686–13690; *Angew. Chem.* **2018**, *130*, 13876–13881.
[46] C. Chen, B. Corry, L. Huang, N. Hildebrandt, *J. Am. Chem. Soc.* **2019**, *141*, 11123–11141.
[47] J. Guo, C. Mingoes, X. Qiu, N. Hildebrandt, *Anal. Chem.* **2019**, *91*, 3101–3109.
[48] J. Xu, J. Guo, N. Golob-Schwarzl, J. Haybaeck, X. Qiu, N. Hildebrandt, *ACS Sens.* **2020**, *5*, 1768–1776.
[49] X. Qiu, N. Hildebrandt, *ACS Nano* **2015**, *9*, 8449–8457.

Manuscript received: June 23, 2022
Revised manuscript received: July 14, 2022
Accepted manuscript online: July 15, 2022
Version of record online: July 29, 2022